Doppler-free dual-comb spect using optical-optical double technique

doi: 10.1364/OE.24.025894

Research Article | Vol. 24, No. 22 | 31 Oct 2016 | OPTICS EXPRESS 25894
Optics EXPRESS

Doppler-free dual-comb spectroscopy of Rb using optical-optical double resonance technique

AKIKO NISHIYAMA,[1,2,3] SATORU YOSHIDA,[1,2] YOSHIAKI NAKAJIMA,[1,2] HIROYUKI SASADA,[2,4] KEN'ICHI NAKAGAWA,[1] ATSUSHI ONAE,[2,5] AND KAORU MINOSHIMA[1,2,*]

[1]*Department of Engineering Science, Graduate School of Informatics, University of Electro-Communications (UEC), 1-5-1 Chofugaoka, Chofu, Tokyo 182-8585, Japan*
[2]*Japan Science and Technology Agency (JST), ERATO MINOSHIMA Intelligent Optical Synthesizer (IOS) Project, 1-5-1 Chofugaoka, Chofu, Tokyo 182-8585, Japan*
[3]*Research Fellow of the Japan Society for the Promotion of Science (JSPS), 1-5-1 Chofugaoka, Chofu, Tokyo 182-8585, Japan*
[4]*Department of Physics, Faculty of Science and Technology, Keio University, 3-14-1, Hiyoshi Kohoku-ku, Yokohama 223-8522, Japan*
[5]*National Metrology Institute of Japan (NMIJ), National Institute of Advanced Industrial Science and Technology (AIST), 1-1-1, Umezono, Tsukuba, Ibaraki, 305-8563, Japan*
[*]*k.minoshima@uec.ac.jp*

Abstract: We present a Doppler-free high-resolution dual-comb spectroscopy technique in which a dual-comb system is employed to perform optical-optical double-resonance (OODR) spectroscopy. In our experimental study, Doppler-free high-resolution and high-frequency-accuracy broadband measurements were realized using the proposed OODR dual-comb spectroscopic technique, which does not require high-power-per-mode frequency combs. We observed fully resolved hyperfine spectra of $5P_{3/2}$ - $4D_{5/2}$, $4D_{3/2}$ transitions of Rb at 1530 nm and precisely determined the absolute frequencies of the transitions, with an uncertainty of less than 1 MHz. The variations of the OODR spectral line shapes due to power broadening and alignment and the effects of polarization on the dual-comb OODR spectra were also analyzed. This study provides a widely applicable technique for Doppler-free dual-comb spectroscopy of various gaseous species.

OCIS codes: (300.6320) Spectroscopy, high-resolution; (140.4050) Mode-locked lasers; (300.6210) Spectroscopy, atomic.

References and links

1. M. J. Thorpe, D. Balslev-Clausen, M. S. Kirchner, and J. Ye, "Cavity-enhanced optical frequency comb spectroscopy: application to human breath analysis," Opt. Express **16**(4), 2387–2397 (2008).
2. S. A. Diddams, L. Hollberg, and V. Mbele, "Molecular fingerprinting with the resolved modes of a femtosecond laser frequency comb," Nature **445**(7128), 627–630 (2007).
3. P. Maslowski, K. F. Lee, A. C. Johansson, A. Khodabakhsh, G. Kowzan, L. Rutkowski, A. A. Mills, C. Mohr, J. Jiang, M. E. Fermann, and A. Foltynowicz, "Surpassing the path-limited resolution of Fourier-transform spectrometry with frequency combs," Phys. Rev. A **93**(2), 021802 (2016).
4. J. Mandon, G. Guelachvili, and N. Picqué, "Fourier transform spectroscopy with a laser frequency comb," Nat. Photonics **3**(2), 99–102 (2009).
5. I. Coddington, W. C. Swann, and N. R. Newbury, "Coherent multiheterodyne spectroscopy using stabilized optical frequency combs," Phys. Rev. Lett. **100**(1), 013902 (2008).
6. I. Coddington, W. C. Swann, and N. R. Newbury, "Coherent linear optical sampling at 15 bits of resolution," Opt. Lett. **34**(14), 2153–2155 (2009).
7. I. Coddington, N. Newbury, and W. Swann, "Dual-comb spectroscopy," Optica **3**(4), 414–426 (2016).
8. W. Demtröder, *Laser Spectroscopy*, 4th ed. (Springer, 2008), Vol. 2.
9. D. C. Heinecke, A. Bartels, T. M. Fortier, D. A. Braje, L. Hollberg, and S. A. Diddams, "Optical frequency stabilization of a 10 GHz Ti:sapphire frequency comb by saturated absorption spectroscopy in ^{87}rubidium," Phys. Rev. A **80**(5), 053806 (2009).
10. S. Y. Zhang, J. T. Wu, Y. L. Zhang, J. X. Leng, W. P. Yang, Z. G. Zhang, and J. Y. Zhao, "Direct frequency comb optical frequency standard based on two-photon transitions of thermal atoms," Sci. Rep. **5**, 15114 (2015).
11. A. Hipke, S. A. Meek, G. Guelachvili, T. W. Hänsch, and N. Picque, "Doppler-free broad spectral bandwidth two-photon spectroscopy with two laser frequency combs," in *Conference on Lasers and Electro Optics* (Optical Society of America, 2013), paper CTh5C.8.

#276244 http://dx.doi.org/10.1364/OE.24.025894
Journal © 2016 Received 20 Sep 2016; revised 24 Oct 2016; accepted 25 Oct 2016; published 28 Oct 2016

Optics EXPRESS

12. N. Kuse, A. Ozawa, I. Ito, and Y. Kobayashi, "Dual-comb saturated absorption spectroscopy," in *Conference on Lasers and Electro Optics* (Optical Society of America, 2013), paper CTu2I.1.
13. A. Nishiyama, D. Ishikawa, and M. Misono, "High resolution molecular spectroscopic system assisted by an optical frequency comb," J. Opt. Soc. Am. B **30**(8), 2107–2112 (2013).
14. A. Nishiyama, K. Nakashima, A. Matsuba, and M. Misono, "Doppler-free two-photon absorption spectroscopy of rovibronic transition of naphthalene calibrated with an optical frequency comb," J. Mol. Spectrosc. **318**, 40–45 (2015).
15. B. Spaun, P. B. Changala, D. Patterson, B. J. Bjork, O. H. Heckl, J. M. Doyle, and J. Ye, "Continuous probing of cold complex molecules with infrared frequency comb spectroscopy," Nature **533**(7604), 517–520 (2016).
16. S. Kasahara, C. Fujiwara, N. Okada, H. Katô, and M. Baba, "Doppler-free optical-optical double resonance polarization spectroscopy of the $^{39}K^{85}Rb$ $1^1\Pi$ and $2^1\Pi$ states," J. Chem. Phys. **111**(19), 8857–8866 (1999).
17. H. Wang, X. T. Wang, P. L. Gould, and W. C. Stwalley, "Optical-optical double resonance photoassociative spectroscopy of ultracold ^{39}K atoms near highly excited asymptotes," Phys. Rev. Lett. **78**(22), 4173–4176 (1997).
18. H. Sasada, "Wavenumber measurements of sub-Doppler spectral lines of Rb at 1.3 μm and 1.5 μm," IEEE Photonics Technol. Lett. **4**(11), 1307–1309 (1992).
19. M. Breton, P. Tremblay, C. Julien, N. Cyr, M. Têtu, and C. Latrasse, "Optically pumped rubidium as a frequency standard at 196 THz," IEEE Trans. Instrum. Meas. **44**(2), 162–165 (1995).
20. M. Breton, N. Cyr, P. Tremblay, M. Têtu, and R. Boucher, "Frequency locking of a 1324 nm DFB laser to an optically pumped rubidium vapor," IEEE Trans. Instrum. Meas. **42**(2), 162–166 (1993).
21. B. Yang, Q. Liang, J. He, T. Zhang, and J. Wang, "Narrow-linewidth double-resonance optical pumping spectrum due to electromagnetically induced transparency in ladder-type inhomogeneously broadened media," Phys. Rev. A **81**(4), 043803 (2010).
22. H. R. Gray and C. R. Stroud, Jr., "Autler-Townes effect in double optical resonance," Opt. Commun. **25**(3), 359–362 (1978).
23. S. Krishnamurthy, Y. Wang, Y. Tu, S. Tseng, and M. S. Shahriar, "Optically controlled polarizer using a ladder transition for high speed Stokesmetric imaging and quantum zeno effect based optical logic," Opt. Express **21**(21), 24514–24531 (2013).
24. S. Okubo, Y.-D. Hsieh, H. Inaba, A. Onae, M. Hashimoto, and T. Yasui, "Near-infrared broadband dual-frequency-comb spectroscopy with a resolution beyond the Fourier limit determined by the observation time window," Opt. Express **23**(26), 33184–33193 (2015).
25. P. R. Griffiths and J. A. de Haseth, *Fourier Transform Infrared Spectrometry*, 2nd ed. (Wiley, 2007).
26. Y. Nakajima, H. Inaba, K. Hosaka, K. Minoshima, A. Onae, M. Yasuda, T. Kohno, S. Kawato, T. Kobayashi, T. Katsuyama, and F.-L. Hong, "A multi-branch, fiber-based frequency comb with millihertz-level relative linewidths using an intra-cavity electro-optic modulator," Opt. Express **18**(2), 1667–1676 (2010).
27. W.-K. Lee and H. S. Moon, "Measurement of absolute frequencies and hyperfine structure constants of $4D_{5/2}$ and $4D_{3/2}$ levels of ^{87}Rb and ^{85}Rb using an optical frequency comb," Phys. Rev. A **92**(1), 012501 (2015).
28. H. S. Moon, L. Lee, and J. B. Kim, "Double-resonance optical pumping of Rb atoms," J. Opt. Soc. Am. B **24**(9), 2157–2164 (2007).
29. Y. Yoshikawa, T. Umeki, T. Mukae, Y. Torii, and T. Kuga, "Frequency stabilization of a laser diode with use of light-induced birefringence in an atomic vapor," Appl. Opt. **42**(33), 6645–6649 (2003).

1. Introduction

Optical frequency combs are advantageous as spectroscopic light sources due to their broadband spectra consisting of dense, narrow optical frequency modes whose absolute frequencies can be precisely determined. Comb-mode-resolved spectroscopies, such as VIPA (virtually imaged phased array)-based spectroscopy [1,2], Fourier-transform spectroscopy (FTS) [3,4] and dual-comb spectroscopy [5–7], provide broadband, high-resolution spectra thanks to the narrow linewidths of the comb modes. However, the actual resolution of direct comb spectroscopies have been limited in almost all previous studies due to Doppler broadening. In the spectroscopy of gaseous species, it is necessary to adopt Doppler-free techniques [8] to achieve sub-Doppler resolution.

In previous studies of Doppler-free direct comb spectroscopy, saturated absorption spectroscopy was demonstrated by using a high-mode-power, high-repetition-rate comb [9], and Doppler-free two-photon transitions, which were introduced by several pairs of comb lines, were observed [10]. Although a few dual-comb spectroscopy studies have also been performed [11,12], and demonstrating the use of dual-combs in nonlinear Doppler-free spectroscopy, these techniques have not been widely applied in molecular or atomic spectroscopy in spite of growth in the use of dual-comb spectroscopy. It is because the direct use of combs in nonlinear Doppler-free spectroscopies has a drawback, namely, the low powers of the individual comb modes. As the high-resolution spectroscopic light source, thus, frequency-tunable continuous wave (cw) lasers are still

Optics EXPRESS

in use although the significant time and effort are required to conduct the measurement of broadband molecular spectra [13,14].

Recently, Doppler-reduced direct comb FTS using buffer gas cooling technique has been reported, and revealed detailed rovibrational structures of some molecular species [15]. Because the velocity-selective spectroscopies, such as buffer gas cooling, molecular beam, double resonance spectroscopies, are based on linear detection, they are advantageous for direct comb Doppler-free spectroscopies with low power per mode. In this study, we combined dual-comb spectroscopy with Doppler-free optical-optical double resonance (OODR) spectroscopy for the first time. OODR spectroscopy is a Doppler-free velocity-selective spectroscopy with a cw pump laser, and widely used in the field of high-resolution molecular and atomic spectroscopies [16–20]. By applying OODR technique to dual-comb spectroscopy, Doppler-free dual-comb spectroscopy is applicable to various gaseous species by full use of narrow linewidths of comb modes. As a demonstration of dual-comb OODR spectroscopy, we observed the OODR spectra of the $5P_{3/2}$ - $4D_{5/2}$, $4D_{3/2}$ transitions of Rb and precisely determined the absolute frequencies of the spectra. The line shapes of the Doppler-free spectra were analyzed in detail, and the results obtained by employing polarization OODR spectroscopy to observe the same transition were compared with those of dual-comb OODR spectroscopy. Finally, the effects of polarization on the dual-comb OODR spectroscopy results were determined. Through these detailed studies, dual-comb OODR spectroscopy is established and provides widely applicable tool for Doppler-free comb spectroscopy.

2. Principles

Figure 1(a) depicts the energy diagram of ^{87}Rb, showing the ladder-type OODR transitions [18,19]. The OODR spectroscopy is based on velocity-selective optical pumping as illustrated in Fig. 1(b), if a pump laser linewidth is small and the laser frequency equals the transition frequency to an intermediate state, only atoms with velocities near zero are optically excited from the ground state which has a thermal velocity distribution. Doppler-free OODR signals are detected as probe laser absorptions caused by only the atoms in the intermediate state. In our spectroscopic system, the 780 nm (D2 line) $5S_{1/2}$ - $5P_{3/2}$ transition is pumped by a narrow-linewidth cw laser, and the 1530 nm transitions to $4D_{5/2}$ and $4D_{3/2}$ from $5P_{3/2}$ are probed simultaneously by using the dual-comb technique.

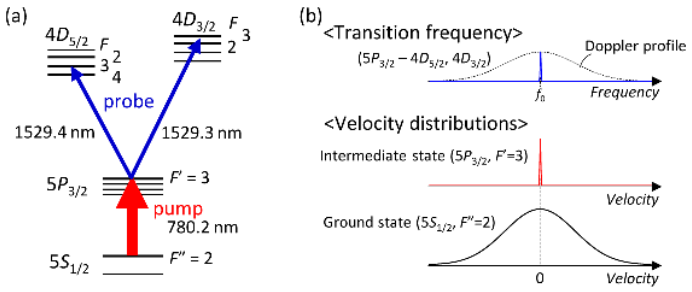

Fig. 1. (a) Energy level diagram for ^{87}Rb. Pump laser excites $5S_{1/2}$ - $5P_{3/2}$ transition, and dual-comb spectroscopy is used to measure transitions to $4D_{5/2}$ and $4D_{3/2}$ states. (b) Principle of OODR spectroscopy.

A linewidth of OODR spectrum is determined by natural widths of the transitions, the laser linewidths, and power broadening. The spectral linewidth (Γ_{OODR}) without power broadening can be calculated for the case in which the pump and probe lasers are in a co-propagating configuration, and can be expressed as follows [20]:

$$\Gamma_{OODR} = \frac{\nu_{comb}}{\nu_{pump}}\left(\Gamma_i + \Delta\nu_{pump}\right) + \left(\Gamma_i + \Gamma_f + \Delta\nu_{comb}\right), \quad (1)$$

where ν_{pump} and ν_{comb} are the frequencies of the pump laser and signal comb modes, respectively; $\Delta\nu_{pump}$ and $\Delta\nu_{comb}$ are the corresponding laser linewidths; and Γ_i and Γ_f are

Optics EXPRESS

the natural linewidths of the $5S_{1/2}$ - $5P_{3/2}$ and $5P_{3/2}$ - $4D_{5/2}$ transitions and equal 6 MHz and 2 MHz, respectively.

In the case that the lasers are in a counter-propagating configuration, observable OODR linewidth is narrower than the one observed with co-propagating lasers due to the effect of electromagnetically induced transparency [21]. In addition, Autler-Townes splitting which was AC stark effect induced by the pump laser is observable when we use higher pump power [22,23]. The splitting is submerged in co-propagating configuration by the Doppler-effect.

3. Experiment

3.1 Spectroscopic system setup

Figure 2 is a schematic diagram of the dual-comb OODR spectroscopic system. The pump laser is an extended-cavity diode laser (ECDL) with an emitted radiation linewidth of less than 1 MHz. The absolute frequency of the ECDL is locked to a hyperfine (D2 line) Rb transition by using saturated absorption spectroscopy with the frequency modulation technique and lock-in detection. A 5-cm-long Rb gas cell serves both as a reference for the pump laser and as an OODR spectroscopy sample. The cell is heated to 70°C and filled with ^{85}Rb and ^{87}Rb isotopes, which were mixed according to their natural abundances.

The dual-comb system employed in this study consists of two homemade mode-locked Er-doped fiber lasers with center wavelengths of 1560 nm and slightly different repetition frequencies of about 56.6 MHz. These lasers are employed as signal and local combs. The signal comb and pump laser outputs overlap and pass through the sample cell. Transmission of the signal comb output interfere with the local comb output. The two comb outputs are filtered by an optical band-pass filter (BPF) with a center wavelength of about 1530 nm and a full-width at half-maximum (FWHM) of 1.1 nm and are then input into a photo detector. The signals are digitized synchronously at the repetition frequency of the local comb ($f_{rep,L}$) by a 14 bits digitizer. The spectra are obtained by taking the fast Fourier-transforms (FFTs) of the averaged interferograms. In each spectrum, the frequency interval between sampling points is determined by the repetition frequency of the signal comb ($f_{rep,S}$). To obtain higher-resolution than the frequency interval, the mode frequencies of the signal comb are scanned by varying $f_{rep,S}$. The averaged interferograms corresponding to the different values of $f_{rep,S}$ are stored in a computer.

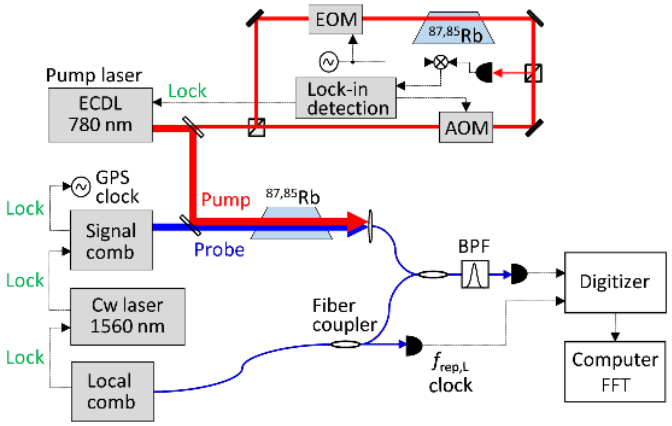

Fig. 2. Schematic diagram of OODR dual-comb system. ECDL: External-cavity diode laser, EOM: Electro-optic modulator, AOM: Acousto-optic modulator, BPF: Optical band-pass filter.

Optics EXPRESS

3.2 Phase-lock scheme and averaging

The phase-lock scheme of the two combs is based on [24]. $f_{rep,S}$ and the offset frequencies of the signal and local combs ($f_{ceo,S}$ and $f_{ceo,L}$, respectively) are phase-locked to radio frequency (RF) signals referencing a global-positioning-system (GPS)-disciplined clock. To achieve a long coherence time, in other words, to obtain a narrow relative linewidth between the two combs, the local comb has an intra-cavity electro-optical modulator (EOM), which enables high-speed control of the effective cavity length. A mode of the local comb is phase-locked to a cw laser at 1560 nm, and the cw laser is locked to a signal comb mode. The cw laser also enables high-speed control by applying feedback to the injection current.

In this study, difference between the repetition frequencies (Δf_{rep}) of two combs is set to approximately 500 Hz, corresponding to an interferogram acquisition time of 1/500 s. The relationships between the repetition frequencies and offset frequencies are fixed as $f_{rep,S}/\Delta f_{rep} = M$ and $f_{ceo,S} = f_{ceo,L}$, respectively, where M is an integer. Even when $f_{rep,S}$ is changed, M is held constant. Based on the relations between their parameters, the digitized interferograms are coherently averaged over 0.1 s. The phase locked dual-comb system has enough coherence in this term. In addition, long-term averaging is achieved by employing phase-correction software [25], which corrects the relative carrier phase drift introduced by the differential phase noise between the two optical paths.

3.3 Evaluation of the relative and absolute laser linewidths

The dual-comb scheme have realized enough performance as reported in [24]. Here, we show that the scheme provides coherence time as long as a dual-comb scheme using ultra-narrow-linewidth cw lasers [5–7]. We evaluated the relative linewidth between the stabilized signal and local combs by measuring the heterodyne beat between another cw laser at 1550 nm (slave laser) and each comb mode [26]. The evaluation method is illustrated schematically in Fig. 3(a). An RF mixer removed common noise attributed to the slave laser, and an FFT analyzer with a 1 mHz resolution and 1000 s measurement time recorded the relative beat spectrum, which is depicted in Fig. 3(b). The FWHM of the observed relative beat spectrum was 2.6 mHz. This result indicates that long coherence times can be obtained using the dual-comb systems [6]. In this measurement, fiber branches used for the beat frequency measurements were covered by sheets to reduce the fiber fluctuations. In practical dual-comb measurement, coherently averaging time is limited by the fiber fluctuation noises, and the coherence time is varied by experimental environments.

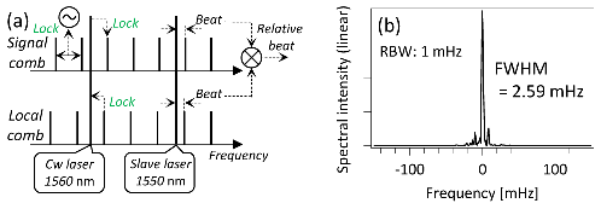

Fig. 3. (a) Schematic of setup used to measure relative beat between relatively stabilized signal and local combs. (b) Relative beat spectrum measured by FFT network analyzer.

We then measured the absolute linewidth of the signal comb mode ($\Delta\nu_{comb}$) to estimate the resolution of our dual-comb OODR spectroscopic system. We measured the relative beat between the signal comb (Signal comb 1) and another comb (Signal comb 2) in the manner depicted in Fig. 3(a) (Fig. 4 (a)). The laser oscillators had the same design and configuration, and the repetition and offset frequencies of each comb were locked to respective RF synthesizers independently. An RF spectrum analyzer with a 300 Hz resolution recorded the relative beat spectrum, which is presented in Fig. 4(b) and exhibits a linewidth of 20.5 kHz. The spectral linewidth can be interpreted as the square root of the sum of the squares of the individual linewidths. Based on the obtained spectral linewidth, the signal-comb-mode linewidth was estimated to be 14.5 kHz. The absolute

Optics EXPRESS

linewidth of the signal comb mode is sufficiently narrow for the measurements performed in this study. In applications requiring higher resolutions, one or two ultra-narrow-linewidth lasers should be employed as reference lasers.

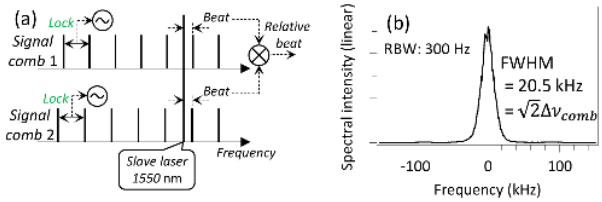

Fig. 4. (a) Schematic of setup used to measure relative beat between signal comb (Signal comb 1) and another RF-stabilized comb (Signal comb 2). Repetition and offset frequencies of each comb were locked to RF signals independently. (b) Relative beat spectrum between independently stabilized combs. RF-stabilized comb mode linewidth ($\Delta\nu_{comb}$) was derived from observed beat spectrum linewidth.

4. Results and discussion

4.1 Observed spectra and absolute frequencies

Figures 5(a) and 5(b) show the center burst and total time span, respectively, of an interferogram obtained by averaging over 200 s. The envelope of the slow free-induction decay signal is observable in Fig. 5(b). Figure 5(c) depicts a spectrum resulting from taking the FFTs of the interferograms acquired every $f_{rep,S}$, which was initially 56 604 500 Hz and was scanned to 56 604 516 Hz in 1 Hz increments. The equivalent scan step of the optical frequency modes at 1530 nm was about 3.5 MHz. The horizontal axis was determined by the absolute signal comb mode frequencies for each $f_{rep,S}$. The spectral envelope represents the transmission profile of the optical BPF employed in this study. In the spectrum, the absorptions corresponding to the transitions to the $4D_{5/2}$ and $4D_{3/2}$ states from the intermediate state appear at 196.024 THz and 196.037 THz, respectively. The absolute frequency of pump laser was locked to a hyperfine transition of ^{87}Rb, $5S_{1/2}$ (F''= 2) - $5P_{3/2}$ (F'= 3). The pump power was 1 mW, and the beam diameter was about 2 mm. The pump laser and signal comb outputs were linearly polarized in parallel.

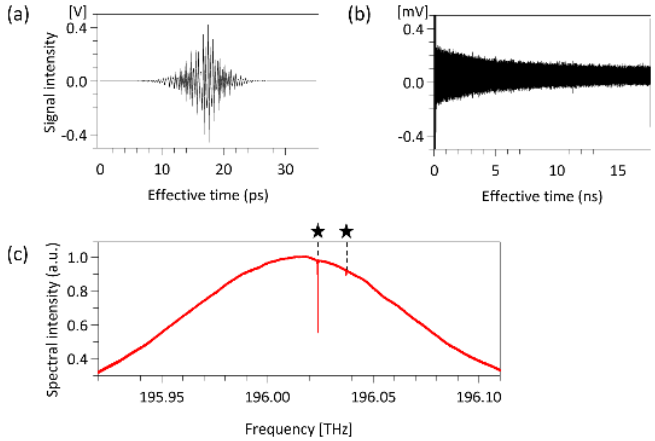

Fig. 5. Observed interferogram obtained by averaging over 200 s. Magnified views of (a) center burst signal and (b) free-induction decay. (c) Spectrum (195.92-196.11 THz) obtained from FFTs of 17 interferograms. Absorptions corresponding to $5P_{3/2}$ - $4D_{5/2}$ and $5P_{3/2}$ - $4D_{3/2}$ transitions are observable.

Magnified views of the normalized absorption spectra of the $5P_{3/2}$ (F'= 3) - $4D_{5/2}$ and $5P_{3/2}$ (F' = 3) - $4D_{3/2}$ transitions are shown in Figs. 6(a) and 6(b), respectively. A reference spectrum was recorded using the same conditions without the pump beam and was employed to obtain a baseline for the normalization. In Figs. 6, the vertical blue lines

Optics EXPRESS

and circles along the tops of the graphs denote the absolute frequencies of the hyperfine transitions that were reported in [27], and the transition assignments are shown above the graphs. Three hyperfine transitions are allowed in the $5P_{3/2}$ (F' = 3) - $4D_{5/2}$ transition, and two transitions are allowed in the $5P_{3/2}$ (F' = 3) - $4D_{3/2}$ transition by the ΔF = 0, ± 1 selection rule. In Fig. 6(a), the strongest resonance, with approximately 75% absorption, is evident because the $5P_{3/2}$ (F' = 3) - $4D_{5/2}$ (F'' = 4) transition is a cycling transition. On the other hand, weak, but fully resolved hyperfine transitions were observed in Fig. 6(b).

These spectra were fitted to Lorentz functions. The two weak absorption lines in the $5P_{3/2}$ (F' = 3) - $4D_{5/2}$ (F = 3 and 2 in Fig. 6(a)) were fitted by fixing parameters of the center frequencies to the values reported in [27] due to the difficulty of fitting weak transitions. The other parameters were fitted to the observed spectra. These fitted Lorentz functions and residuals are also depicted in Figs. 6. As shown, the observed spectra agree closely with the Lorentzian profiles. The FWHMs of the fitted Lorentz functions for the $5P_{3/2}$ (F' = 3) - $4D_{5/2}$ (F = 4) and $5P_{3/2}$ (F' = 3) - $4D_{3/2}$ (F = 3) transitions are 45.5 MHz and 35.5 MHz, respectively. These results indicate that Doppler-free high-resolution measurements below the repetition frequencies of the combs were achieved.

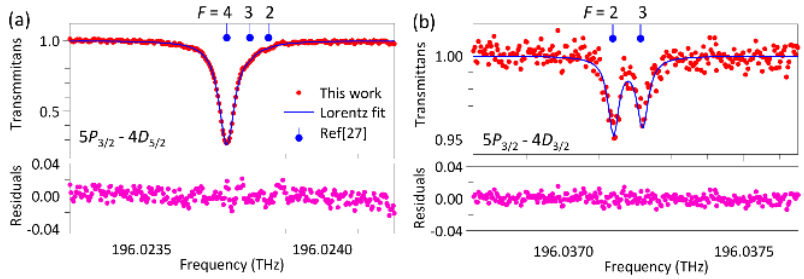

Fig. 6. Normalized OODR spectra and fitted Lorentz functions of (a) $5P_{3/2}$ - $4D_{5/2}$ transition (196.0233-196.0242 THz) and (b) $5P_{3/2}$ - $4D_{3/2}$transition (196.03675-196.03765 THz) of ^{87}Rb. Transition frequencies reported in [27] are shown by vertical lines and circles. Hyperfine transition assignments are presented above the graphs.

The center frequencies of the fitted Lorentz functions are listed in the second column of Table 1 for the $5P_{3/2}$ (F' = 3) - $4D_{5/2}$ (F = 4) transition of ^{87}Rb, and the $5P_{3/2}$ (F' = 4) - $4D_{5/2}$ (F = 5) transition of ^{85}Rb, which is also a cycling transition. For the ^{85}Rb measurements, the pump laser was locked to the hyperfine transition $5S_{1/2}$ (F'' = 3) - $5P_{3/2}$ (F' = 4), and the other parameters were same as those used to measure ^{87}Rb. The standard deviations (δ) of the center frequencies of the fits are shown in the third column of Table 1. These deviations depend on the signal-to-noise ratios (SNRs) of the observed spectra and are less than 100 kHz. The $5P_{3/2}$ - $4D_{3/2}$ transitions, whose measurements are not included in Table 1, have δ values on the order of a few megahertz because of their low SNRs. The fourth column lists the results obtained previously by Lee et al. by using double resonance optical pumping (DROP) spectroscopy with frequency-comb-referenced cw lasers [27], and the values in parentheses represent the measurement uncertainties. The differences between the previous measurements and ours are less than 1 MHz.

Table 1. Absolute Frequencies of Observed Spectra in This Work and Previous Work[a]

Transition	This work (MHz)	δ (kHz)	W.-K. Lee et al. [27] (MHz)	Difference (MHz)
^{87}Rb, $5P_{3/2}$ (F' = 3) - $4D_{5/2}$ (F = 4)	196 023 735.47	78	196 023 735.290 (42)	0.18
^{85}Rb, $5P_{3/2}$ (F' = 4) - $4D_{5/2}$ (F = 5)	196 023 776.26	93	196 023 776.715 (47)	–0.46

[a]The third column (δ) shows standard deviations of the center frequencies of the fittings. Total uncertainty of this work was discussed in the main text.

We then estimated the uncertainty of our absolute frequency measurements. The first source of uncertainty in our dual-comb spectroscopic system was the uncertainty of the RF-stabilized signal comb modes. The RF signals were referenced to a GPS disciplined

Optics EXPRESS

clock with an uncertainty of 3×10^{-12} in 1 s, corresponding to a stabilized comb mode uncertainty of 0.6 kHz at 196 THz. The second cause of uncertainty was deviation of the pump laser frequency, which was locked to the intermediate state. In these measurements, the pump laser frequency uncertainty was on the order of several hundreds of kilohertz, making it a main source of uncertainty in the obtained OODR spectra. The third contribution to the uncertainty was the SNR of the spectrum. Especially when determining the frequency of a weak absorption, which would have a low SNR, large fitting deviations could occur, making the SNR a dominant source of measurement uncertainty. Longer averaging time or higher gas concentration enable improvement in SNR of the weak transitions. In total, the obtained differences listed in Table 1 between the results of this study and previous studies are within the measurement uncertainty.

4.2 Linewidths and shapes

Linewidth of the OODR spectrum is estimated to be 11.5 MHz by using Eq. (1). In fact, as shown in Figs. 6, the observed spectral widths are broader than this estimated width due to the power broadening caused by the pump laser. Since the power of the probe laser, which was equal to that of a signal comb mode, was on the order of nanowatts, its power broadening effect was negligible. Figure 7(a) shows the dependence of the OODR spectrum on the pump power in the $5P_{3/2}$ (F' = 3) - $4D_{5/2}$ transition of ^{87}Rb. The pump power was changed from 0.2 mW to 4 mW. Each spectrum was obtained by 50 s averaging with 3.5 MHz scan steps. The FWHMs of Lorentzian fits to the $5P_{3/2}$ (F' = 3) - $4D_{5/2}$ (F = 4) transition are plotted in Fig. 7(b) versus the pump power, clearly illustrating the dependence of the FWHM on the pump power. Even when the pump power is only 0.2 mW, the FWHM is 19.9 MHz due to power broadening. As described in [28], the large transition dipole moment is attributed to the significant effect of power broadening on this transition.

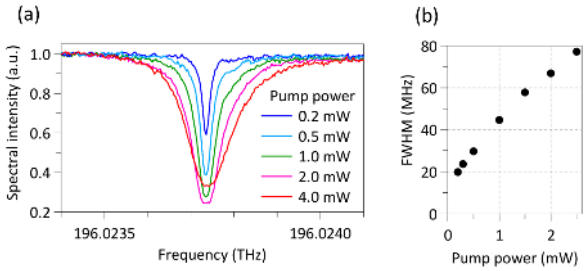

Fig. 7. (a) Variation of spectral line shape of $5P_{3/2}$ (F' = 3) - $4D_{5/2}$ transition with pump power. (b) FWHM of $5P_{3/2}$ (F' = 3) - $4D_{5/2}$ (F = 4) spectrum versus pump laser power.

Next, we changed the alignment of the pump beam and the signal comb output to a counter-propagating configuration. When the pump power was less than 0.5 mW, the frequency scan step of the modes were 1.75 MHz. In the measurements with higher pump powers, the averaging time and scan step were same those used to obtain Fig. 7(a). Figure 8(a) shows the dependence of the spectrum of the $5P_{3/2}$ (F' = 3) - $4D_{5/2}$ transition on the pump laser power. At low pump powers, the spectra are narrow as mentioned in Principles. The spectra have shapes that closely agree with Lorentz functions, and observed linewidth in this study at pump powers of 0.2 mW and 0.1 mW are 9.5 MHz and 6.6 MHz, respectively. The linewidth results are same order of previous works of DROP spectroscopies with cw lasers [28].

Optics EXPRESS

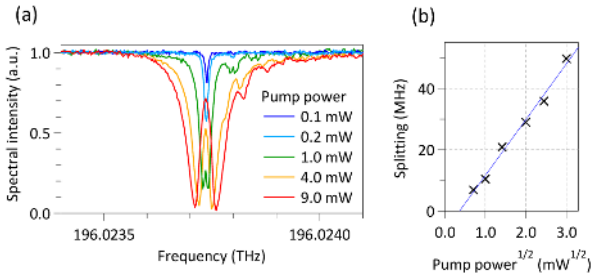

Fig. 8. (a) $5P_{3/2}$ (F' = 3) - $4D_{5/2}$ transition spectra obtained using counter-propagating beams and various pump powers. (b) Splitting introduced by Autler-Townes effect versus square root of pump laser power. Blue line represents linear fit.

It was difficult to fit the spectra obtained using higher pump powers to Lorentz functions because of the Autler-Townes splitting that appears and becomes more prominent with increasing pump power. The splitting shows linear dependence on the electric field (pump power$^{1/2}$), which closely agrees with the behavior expected due to this effect [22]. The differences between the measured distances and the linear fit are less than the scan step range used to perform these measurements (Fig. 8(b)).

4.3 Polarization effect

In this section, we discuss the effects of polarization on dual-comb OODR spectra. Figure 9 presents the $5P_{3/2}$ (F' = 3) - $4D_{5/2}$ spectrum obtained using a circularly polarized pump laser in the co-propagating configuration. The pump laser power was 1 mW, the probe laser was linearly polarized, and the averaging time was 200 s. Although the spectra in Figs. 6(a) and 9 correspond to the same transition, that in Fig. 9 could not be fitted by Lorentz functions with the same fitting parameters due to its asymmetry. In our dual-comb OODR spectroscopy results, we observed a variety of asymmetric profiles when the pump laser was not linearly polarized, while asymmetry has not been reported in spectra obtained using pairs of cw lasers [18,19].

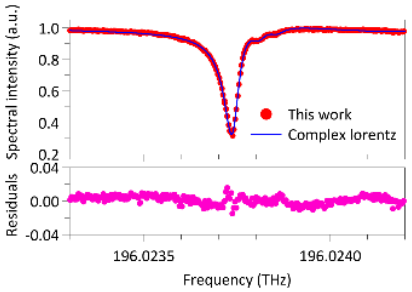

Fig. 9. OODR spectrum of $5P_{3/2}$ - $4D_{5/2}$ transition obtained using circularly polarized pump laser.

Light-induced birefringence is expected to contribute to the observed asymmetry. Circularly polarized pump beams, with polarizations of σ^+ or σ^-, introduce only $\Delta m = +1$ or -1 transitions, respectively. Therefore, degenerate m sublevels in the intermediate state are selectively populated. In this case, the absorption coefficients of the σ^+- and σ^--polarized beams are not the same. The polarized atoms rotate the polarization of the probe laser, which is equivalent to the principle of polarization spectroscopy [29]. To confirm the polarization effect, we performed polarization OODR spectroscopy using the setup shown in Fig. 10(a). The probe beam was transmitted through a $\lambda/2$ plate and a polarizer, and the polarization change was detected by measuring the spectral intensity. The spectrum of the $5P_{3/2}$ (F' = 3) - $4D_{5/2}$ transition was obtained using a 1 mW circularly polarized pump laser and linearly polarized signal comb. This spectrum is presented in Fig. 10(b), which shows the shape of the dispersive resonance.

Optics EXPRESS

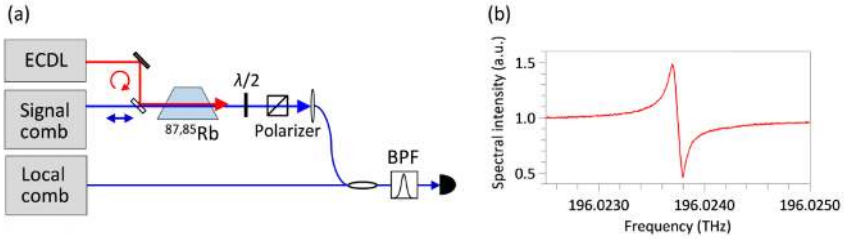

Fig. 10. (a) Experimental setup for polarization dual-comb OODR spectroscopy. (b) Polarization OODR spectrum of $5P_{3/2}$ (F' = 3) - $4D_{5/2}$ transition.

Based on the polarization dual-comb OODR spectroscopy results, we concluded that the asymmetry in Fig. 9 is attributable to the light-induced birefringence of the intermediate state. In measurements performed using cw lasers, asymmetric spectra have not been detected, because only the absorptions of the cw probe lasers were measured. However, in dual-comb OODR spectroscopy, spectra are obtained based on the interference between two combs; therefore, the polarization changes of the signal comb modes are detected in the interference signals as intensity variations, like in polarization interferometry. Thus, we fitted the spectrum in Fig. 9 to a complex Lorentz function representing the sum of the absorption and dispersion spectra. The fitted complex Lorentz function and residuals are also illustrated in Fig. 9, revealing that the observed OODR spectrum agrees closely with the complex Lorentz function. Thus, our experimental results demonstrate that the investigated dual-comb system is useful in polarization OODR spectroscopy. However, in dual-comb OODR spectroscopy, it is also necessary to eliminate carefully the polarization effects that cause OODR spectrum distortion.

5. Conclusion

In this study, we demonstrated the broadband Doppler-free OODR spectroscopy using a dual-comb system. Doppler broadenings were removed by the velocity-selective pumping, and the dual-comb system was applied as a probe system that can achieve high resolution only limited by the comb mode linewidth of 14.5 kHz.

We measured the $5S_{1/2}$ - $5P_{3/2}$ - $4D_{5/2}$, $4D_{3/2}$ transitions of Rb, and obtained fully resolved hyperfine spectra. The absolute frequencies of the $5P_{3/2}$ (F' = 3) - $4D_{5/2}$ (F = 4) and $5P_{3/2}$ (F' = 4) - $4D_{5/2}$ (F = 5) transitions of ^{87}Rb and ^{85}Rb, respectively, were determined with sub-megahertz uncertainty. In this study, the total uncertainty was limited by that of the cw pump laser frequency, which was stabilized using the frequency of an intermediate state. We observed the spectral width and shape variations with the pump laser power. The effect of power broadening on the measurements obtained with the pump and probe lasers in the co-propagating configuration was significant. In the counter-propagating configuration, Autler-Townes splitting was observed clearly. The narrowest spectral width of 6.6 MHz was obtained in the counter-propagating configuration with 0.1 mW pump power. Additionally, we considered the polarization effect in dual-comb OODR spectroscopy and confirmed that the spectral asymmetry was caused by the light-induced birefringence of the intermediate states that was introduced by the circularly polarized pump laser. Finally, we performed polarization dual-comb OODR spectroscopy and obtained the dispersion spectrum.

By these detailed investigation, the dual-comb OODR spectroscopic technique is established and enables broadband spectroscopic measurements of various gaseous species with Doppler-free high resolutions and high accuracies to be achieved. We expect that dual-comb spectroscopy techniques involving velocity selection, such as double resonance and molecular beam spectroscopy, will be powerful and widely applicable tools that can be employed to perform precise, high-resolution molecular and atomic spectroscopy.

Optics EXPRESS

Funding

Japan Science and Technology Agency (JST) through the ERATO MINOSHIMA Intelligent Optical Synthesizer (IOS) Project and Grant-in-Aid for JSPS Fellows (16J02345).

Acknowledgments

We thank Eiji Tokunaga, Kazuaki Nakata, Naoyuki Shiokawa, and Masayuki Sirakawa (Tokyo University of Science) as well as Akifumi Asahara and Ken'ichi Kondo (UEC) for their assistance in the early stages of developing the Er-doped fiber lasers. We also thank Hajime Inaba and Sho Okubo (AIST) for their valuable advice concerning the dual-comb system setup, and Masaaki Hirano, Yoshinori Yamamoto and Takemi Hasegawa of Sumitomo Electronics Inc. for providing us with highly nonlinear fibers.